BIOCHEMISTRY
including biophysical chemistry & molecular biology
Article

Biochemistry **2011,** *50,* 491–501 491
DOI: 10.1021/bi101883y

High-Resolution Two-Dimensional ^{1}H and ^{14}N Hyperfine Sublevel Correlation Spectroscopy of the Primary Quinone of Photosystem II[†]

Ruchira Chatterjee, Sergey Milikisiyants, Christopher S. Coates, and K. V. Lakshmi*

Department of Chemistry and Chemical Biology and The Baruch '60 Center for Biochemical Solar Energy Research, Rensselaer Polytechnic Institute, Troy, New York 12180, United States

Received November 25, 2010; Revised Manuscript Received December 15, 2010

ABSTRACT: Quinones are naturally occurring isoprenoids that are widely exploited by photosynthetic reaction centers. Protein interactions modify the properties of quinones such that similar quinone species can perform diverse functions in reaction centers. Both type I and type II (oxygenic and nonoxygenic, respectively) reaction centers contain quinone cofactors that serve very different functions as the redox potential of similar quinones can operate at up to 800 mV lower reduction potential when present in type I reaction centers. However, the factors that determine quinone function in energy transduction remain unclear. It is thought that the location of the quinone cofactor, the geometry of its binding site, and the "smart" matrix effects from the surrounding protein environment greatly influence the functional properties of quinones. Photosystem II offers a unique system for the investigation of the factors that influence quinone function in energy transduction. It contains identical plastoquinones in the primary and secondary quinone acceptor sites, Q_A and Q_B, which exhibit very different functional properties. This study is focused on elucidating the tuning and control of the primary semiquinone state, Q_A^-, of photosystem II. We utilize high-resolution two-dimensional hyperfine sublevel correlation spectroscopy to directly probe the strength and orientation of the hydrogen bonds of the Q_A^- state with the surrounding protein environment of photosystem II. We observe two asymmetric hydrogen bonding interactions of reduced Q_A^- in which the strength of each hydrogen bond is affected by the relative nonplanarity of the bond. This study confirms the importance of hydrogen bonds in the redox tuning of the primary semiquinone state of photosystem II.

Quinones display enormous versatility of function in photosynthetic reaction centers (RCs) (*1*). It is known that both type I and type II RCs contain quinones that serve very different functions, as the redox potential of similar quinones can operate at up to 800 mV lower (more negative) reduction potential when present in type I RCs (*1*). Photosystem II (PSII) and photosystem I (PSI) are key examples of type II and type I RCs, respectively, and these systems provide appropriate platforms for investigation of the determinants of quinone function in photosynthetic proteins. PSII contains identical plastoquinone molecules in the primary (Q_A) and secondary (Q_B) site that exhibit very different charge transfer properties; Q_A is a single-electron acceptor, while Q_B is a two-electron, two-proton acceptor that undergoes proton-coupled electron transfer reactions (*2*−*4*). It is thought that the structural differences in the binding site of Q_A and Q_B of PSII lead to the different functional roles of the primary and secondary quinone cofactors.

The recent X-ray crystal structures of PSII provide a glimpse of the interactions of the primary and secondary quinone cofactors with the surrounding protein environment (*2*, *3*, *5*, *6*). For example, in the 3.0 Å resolution X-ray crystal structure of PSII, the quinone ring of Q_A is sandwiched between hydrophobic Trp and Leu residues and the keto oxygen atoms of the quinone are thought to be hydrogen bonded (H-bonded) to the His and Phe/Ala residues of the surrounding protein environment in the D2 polypeptide (*5*) (Figure 5A). Q_B is pseudo-C_2 symmetric to Q_A in PSII. The quinone ring of Q_B interacts with hydrophobic Phe and Leu residues, and Q_B is thought to be H-bonded to the His, Ser, and Phe residues of the surrounding protein in the D2 polypeptide (*5*). In addition, there are headgroups of several lipids in the vicinity of the Q_A and Q_B binding site (*5*). While interactions with the hydrophobic residues are consistent in the various X-ray crystal structures of PSII that have been published to date, there are differences in the orientation of the ring and the isoprenoid chain of Q_A and Q_B that could affect the strength of bonding and nonbonding interactions (*7*).

It has been suggested that the features that tune and control the charge transfer properties of Q_A and Q_B are (i) π-stacking and hydrophobic interactions with amino acid side chains or lipid molecules (*2*, *5*, *8*), (ii) hydrogen bonds with neighboring amino acid residues (*9*), (iii) the presence of the non-heme Fe(II) center in the proximity (*8*), and (iv) the orientation of the isoprenoid tail of the plastoquinone molecule (*7*). In particular, it has been suggested that the presence of a single H-bond could alter the potential of a quinone acceptor to a more oxidizing (higher or more positive) value by 100 mV (*1*). This is because in H-bonds, charge redistribution occurs between the H-bonded partners such that electron density is withdrawn from the quinone ring. This stabilizes the reduced semiquinone state relative to the neutral quinone, thereby increasing the redox potential (*1*). Given the fact that the presence of H-bond(s) to the quinone keto oxygen

[†]This study is supported by the Solar Energy Utilization Program, Office of Basic Energy Sciences, United States Department of Energy (DE-FG02-07ER15903).

*To whom correspondence should be addressed: Department of Chemistry and Chemical Biology, Rensselaer Polytechnic Institute, Troy, NY 12180. Phone: (518) 276-3271. Fax: (518) 276-4887. E-mail: lakshk@rpi.edu.

Published on Web 12/15/2010

atoms could exert a large influence on the redox and charge transfer properties, it is important to determine the number, strength, and geometry of the H-bond(s) to improve our understanding of the functional tuning of the Q_A and Q_B cofactors of PSII.

The X-ray crystal structures of PSII provide information about the location of the Q_A and Q_B cofactors of PSII (*2*, *3*, *5*, *6*); however, it is not possible to directly infer the presence of H-bonds of the quinones in these structures. Further, the X-ray crystal structures of PSII provide information about the structure of the quinone and the surrounding protein environment only in the neutral state. There could be important structural changes in the quinone-binding pocket upon reduction of the neutral quinone to the reduced semiquinone state. High-resolution electron paramagnetic resonance (EPR) spectroscopy methods are uniquely suited to directly probe the presence of H-bonds in the paramagnetic semiquinone states, Q_A^- and Q_B^-, of PSII. More specifically, EPR spectroscopy methods that probe the magnetic interactions of the semiquinone state with surrounding nuclei (e.g., ^{1}H and ^{14}N) provide valuable information about the geometric and electronic nature of H-bonds. Previous one-dimensional (1D) and two-dimensional (2D) ^{14}N electron spin-echo envelope modulation (ESEEM) and ^{1}H electron nuclear double resonance (ENDOR) spectroscopy studies of the Q_A^- semiquinone have suggested the presence of H-bonds from the surrounding protein matrix of PSII (*9*−*15*). In the ^{14}N ESEEM spectroscopy studies, the presence of H-bonds was indirectly inferred from the magnetic interactions of Q_A^- with an amide nitrogen atom of the peptide backbone and an amino nitrogen atom of a His residue. In the ^{1}H ENDOR spectroscopy studies, the presence of H-bonds was based on comparison of the ^{1}H hyperfine interaction parameters that were obtained for Q_A^- with those of the plastosemiquinone radical in vitro (*11*). While ^{1}H ENDOR spectroscopy provides an estimate of the characteristics of the H-bonds of Q_A^-, in these studies it is difficult to resolve electron−nuclear couplings from more than one proton because of the severe overlap of spectral features. In addition, while ^{1}H ENDOR spectroscopy provides an accurate determination of the hyperfine couplings to the intrinsic protons in the Q_A^- state, it is difficult to obtain a quantitative measure of weak through-space electron−nuclear couplings (e.g., H-bonds) as these interactions are highly anisotropic or orientation-dependent in nature.

Here, we utilize 2D ^{1}H hyperfine sublevel correlation (HYSCORE) spectroscopy to directly detect H-bonds to the reduced Q_A^- semiquinone state of PSII and to probe the strength and orientation of these H-bonds. We observe two asymmetric hydrogen bonding interactions of Q_A^- in which the strength of each hydrogen bond is affected by the relative nonplanarity of the bond. We unambiguously assign the identity of the nitrogen atom of each H-bonding partner by the simultaneous application of 2D ^{14}N HYSCORE spectroscopy. In addition, we also study the influence of pH on the H-bond interactions of the Q_A^- semiquinone state. The results described here confirm the importance of H-bonding interactions in the redox tuning of the primary semiquinone state of photosystem II.

MATERIALS AND METHODS

Preparation of Photosystem II Membranes from Spinach. Photosystem II (PSII) membranes were isolated from market spinach using modifications of previously published procedures (*16*). The intact thylakoid membranes that were obtained from market spinach were resuspended in a buffer containing 20 mM *N*-(2-hydroxyethyl)piperazine-*N*′-2-ethanesulfonic acid (HEPES) (pH 7.5), 15 mM sodium chloride (NaCl), 4 mM magnesium chloride ($MgCl_2$), 1 mM sodium 2,2′,2″,2‴-(ethane-1,2-diyldinitrilo) tetraacetate (EDTA), and 1 mg/mL bovine serum albumin (BSA) (pH 7.5). The subchloroplast membranes were isolated from the thylakoids by incubation with Triton X-100 for 20 min at 4 °C in a buffer containing 15 mM NaCl, 20 mM 2-(*N*-morpholino)ethanesulfonic acid (MES), 5 mM $MgCl_2$, 1 mM EDTA, 1 mg/mL BSA, and one pinch of catalase (pH 6.0). The subchloroplast membranes were washed repeatedly with the buffer described above and were resuspended in buffer with Triton X-100. The resulting PSII membranes were washed twice with 20 mM MES (pH 6.0), 15 mM NaCl, and 30% ethylene glycol. The PSII membranes were depleted of manganese by treatment with hydroxylamine hydrochloride ($NH_2OH \cdot HCl$) (*17*) followed by repeated washes with buffer containing 50 mM MES (pH 6.5), 0.4 M sucrose, 15 mM NaCl, 1 mM calcium chloride ($CaCl_2$), and 5 mM EDTA (*17*). The high-spin (electron spin $S = 2$) nonheme iron center, Fe(II), of the Mn-depleted PSII membranes was converted to its low-spin (electron spin $S = 0$) form via incubation of the Mn-depleted PSII membranes with 350 mM KCN in a buffer containing 50 mM MES (pH 6.5), 0.4 M sucrose, 10 mM NaCl, and 5 mM $MgCl_2$ (pH 6.5) for 3.5 h at 4 °C (*18*). The Mn-depleted, CN-treated PSII membranes were resuspended in a buffer containing 50 mM glycine, 0.4 M sucrose, 10 mM NaCl, and 5 mM $MgCl_2$ (pH 9.8) and treated with sodium dithionite under anaerobic conditions to chemically reduce the neutral primary quinone, Q_A, to the reduced semiquinone, Q_A^-, state. This reduction step was also performed in a buffer containing 50 mM MES, 0.4 M sucrose, 10 mM NaCl, and 5 mM $MgCl_2$ (pH 6.5 and 5.5). The PSII preparations and buffer exchanges were repeated several times to ensure reproducibility of the pulsed EPR experiments. The isolation, purification, and treatment procedures of PSII membranes were performed in the dark. The Mn-depleted, CN-treated PSII membranes containing the Q_A^- semiquinone were used for the 2D ^{1}H and ^{14}N hyperfine sublevel correlation (HYSCORE) spectroscopy measurements.

In this study, we treat the PSII membranes with KCN as it does not induce structural perturbations in the Q_A^- binding site. Previous studies have compared the Q_A^- state of Zn-substituted and CN-treated PSII membranes (*9*, *13*, *14*). While there was evidence of structural variations of the Q_A^- binding site of Zn-substituted PSII, these variations were not detected in CN-treated PSII (*14*). The ^{14}N HYSCORE spectrum of Q_A^- of CN-treated PSII is identical to the ^{14}N HYSCORE spectrum of Q_A^- of intact PSII (*19*).

Two-Dimensional (2D) Hyperfine Sublevel Correlation (HYSCORE) Spectroscopy. The EPR spectra were recorded on a custom-built X-band Bruker Elexsys 580 spectrometer. The pulsed EPR measurements were conducted with a dielectric flexline probe ER 4118-MD5 (Bruker BioSpin Corp., Billerica, MA) and a dynamic continuous-flow cryostat CF935, (Oxford Instruments, Oxfordshire, U.K.). All the pulsed EPR spectra were recorded at 30 K.

A conventional four-pulse HYSCORE sequence was used to obtain the ^{14}N HYSCORE spectra (*20*). For the four-pulse HYSCORE sequence, the echo amplitude was measured with the $(\pi/2)_y-\tau-(\pi/2)_y-t_1-(\pi)_y-t_2-(\pi/2)_y-(\text{echo})_x$ pulse sequence with a τ delay of 136 ns and a 8 ns detector gate (which is centered at the maximum of the echo signal); the delays are defined as the difference in the starting point of the pulses. The echo intensity

was measured as a function of t_1 and t_2, where t_1 and t_2 were incremented in steps of 24 ns from their initial values of 32 and 40 ns, respectively. The static magnetic field value and the microwave frequency were 345.7 mT and 9.708 GHz, respectively. Equal amplitude pulses of 8 ns for $\pi/2$ and 16 ns for π were used to record a 256 × 256 matrix. The 8 ns time difference between the initial values of the time delays, t_1 and t_2, was used to take into account the difference in length between the $\pi/2$ and π pulses to obtain symmetric spectra. A 16-step phase cycling procedure was used to eliminate the unwanted echoes and antiechoes with phases of the pulses in the sequence described previously (*21*).

A six-pulse HYSCORE sequence was used to obtain the ^{1}H HYSCORE spectra (*22*, *23*) as the use of a four-pulse HYSCORE sequence resulted in (i) strong suppression of the ^{1}H cross-peaks because of strong signal modulations due to the ^{14}N nuclei and (ii) the presence of unwanted internuclear combination peaks that overlap with the ^{1}H cross-peaks. The cross-suppression effect arises from the fact that the observed HYSCORE signal is a multiplication product of modulation of both strongly modulating nuclei, such as ^{14}N, and weakly modulating nuclei, such as protons (*24*). In this case, the strongly modulating nuclei cause partial or complete suppression of signals from weakly modulating nuclei that are coupled to the same electron spin (*24*). Because hyperfine couplings to the protons are of particular interest in this study, we use a six-pulse ^{1}H HYSCORE sequence (*22*) to alleviate the impact of cross suppression on the presence of the ^{14}N nuclei. Both of the unwanted effects, namely, cross suppression and internuclear cross-peaks, were absent in all the six-pulse HYSCORE experiments, resulting in clearly interpretable proton spectra. However, a six-pulse HYSCORE experiment has significantly decreased sensitivity toward ^{14}N nuclei; therefore, we use a conventional four-pulse sequence to record the 2D ^{14}N HYSCORE spectra.

For the acquisition of the 2D HYSCORE spectra using a six-pulse sequence, the echo amplitude was measured with the $(\pi/2)_y-\tau_1-(\pi)_y-\tau_1-(\pi/2)_x-t_1-(\pi)_x-t_2-(\pi/2)_x-\tau_2-(\pi)_x-\tau_2-(\text{echo})_x$ pulse sequence with a τ_1 delay of 48 ns, a τ_2 delay of 136 ns, and an 8 ns detector gate (which is centered at the maximum of the echo signal); the delays are defined as the difference in the starting point of the pulses. The echo intensity was measured as a function of t_1 and t_2, where t_1 and t_2 were incremented in steps of 24 ns from their initial values of 32 and 40 ns, respectively. The static magnetic field was either 345.7 or 345.8 mT, and the microwave frequency was 9.71 GHz. Equal amplitude pulses of 8 ns for $\pi/2$ and 16 ns for π were used to record a 256 × 256 matrix. The 8 ns time difference between the initial values of the time delays, t_1 and t_2, was used to take into account the difference in length between the $\pi/2$ and π pulses to obtain symmetric spectra. The application of an 8-step phase cycling procedure (*22*) was used to eliminate the unwanted echoes.

For both the 2D HYSCORE spectra recorded using a four-pulse sequence and six-pulse sequence, the echo decay was eliminated by a low-order polynomial baseline correction and tapered with a Gaussian function. Prior to the 2D Fourier transformation, the data was zero filled to a 2048 × 2048 matrix and the magnitude spectra were calculated using the Bruker X-EPR software (Bruker BioSpin Corp.). The spectra are presented as contour plots that were prepared in Matlab R2008a.

Analysis of the 2D ^{1}H HYSCORE Spectra. The three principal components of an electron−nuclear hyperfine tensor can be presented as $(A_x,A_y,A_z) = (a_{iso} - T(1-\delta), a_{iso} - T(1+\delta), a_{iso} + 2T)$, where a_{iso}, T, and δ are the isotropic, dipolar, and rhombic components of the tensor, respectively. In the case of axial symmetry ($\delta = 0$, $A_x = A_y = A_\perp = a_{iso} - T$, $A_z = A_\parallel = a_{iso} + 2T$), the proton cross-peaks (which appear as ridges in powder samples) represent straight line segments when plotted in frequency-squared coordinates (*25*). In this case, the anisotropic and isotropic components of the electron−nuclear hyperfine interaction can be obtained from the slope and the intercept of the ridges (*26*). On the basis of the values of the slope $Q_{\alpha(\beta)}$ and the intercept $G_{\alpha(\beta)}$ that are determined experimentally, the values of a_{iso} and T can be calculated with the following equations (*27*):

$$T = \pm\sqrt{\frac{16}{9[1-Q_{\alpha(\beta)}]}\left[G_{\alpha(\beta)} + \frac{4\nu_I{}^2 Q_{\alpha(\beta)}}{1-Q_{\alpha(\beta)}}\right]} \text{ and}$$

$$a_{iso} = \pm 2\nu_I \frac{1+Q_{\alpha(\beta)}}{1-Q_{\alpha(\beta)}} - \frac{T}{2} \quad (1)$$

To obtain $Q_{\alpha(\beta)}$ and $G_{\alpha(\beta)}$, the frequency-squared coordinates of the points were measured on the median of a ridge corresponding to the highest signal intensity along the direction of the ridges. This is appropriate because processes responsible for the line broadening in the 2D frequency space (e.g., nuclear relaxation, hyperfine strain, and signal apodization) would not affect the position of the signal intensity maximum. Similarly, a small rhombicity, δ, of the hyperfine tensor in the first approximation does not alter the position of the median of the ridge and thus would not affect the quality of the analysis. The measured coordinates were fit with the straight line using a least-squares algorithm that yielded the values of $Q_{\alpha(\beta)}$ and $G_{\alpha(\beta)}$.

In principle, each pair of $Q_{\alpha(\beta)}$ and $G_{\alpha(\beta)}$ values results in four sets of possible hyperfine parameters (see eq 1), where the sign of T can be positive or negative and for a given value of T, there are two possible values of a_{iso}. For the intrinsic protons of the semiquinone radical, the appropriate set of hyperfine values is assigned by comparison to the literature data of the plastosemiquinone anion radical (*11*) and other benzosemiquinone radicals (*27*, *28*). For the hyperfine values of the H-bonds, the sign of T was selected as positive because the value of T is mostly determined by through-space dipolar interactions. The appropriate value of a_{iso} can be determined on the basis that the absolute value of the perpendicular component of the hyperfine tensor is expected to be much smaller than the value of the parallel component and a_{iso} would be relatively small in comparison with the value of T (*29*).

As a final test of the validity of the obtained hyperfine parameters, numerical simulations of the spectra were performed using the *saffron* function of the EasySpin software package (*30*) and the numerical simulations were compared with the experimental spectra.

To estimate the errors of the obtained hyperfine parameters, we measured the admissible variations of values of the slope and the intercept ($Q_{\alpha(\beta)}$ and $G_{\alpha(\beta)}$, respectively) by considering various points in the middle of the ridges, and the variation amplitude of an obtained hyperfine parameter was taken as its error bar.

Analysis of the 2D ^{14}N HYSCORE Spectra. To obtain hyperfine parameters of the ^{14}N nuclei, we performed numerical simulations using the *saffron* function of the EasySpin software package (*30*). The simulated spectra were carefully compared with the experimental ones to match the position of the ridges and

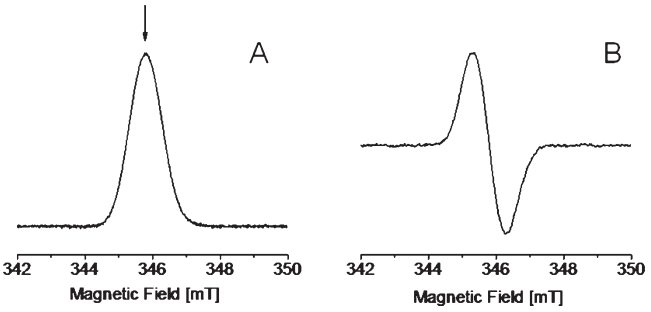

FIGURE 1: (A) Magnetic field sweep electron spin echo spectrum of the reduced Q_A^- semiquinone of PSII at pH 9.8. (B) Derivative line shape of the spin echo spectrum shown in panel A. Indicated by an arrow is the magnetic field position that was used for the measurement of the 2D ^{1}H and ^{14}N HYSCORE spectra.

signal intensity distribution over the different points of the ridges. All hyperfine tensors were assumed to be rhombic with an arbitrary orientation with respect to the quadrupole tensors.

RESULTS

The primary semiquinone anion, Q_A^- (electron spin $S = {}^1/_2$), is magnetically coupled to a proximal high-spin (electron spin $S = 2$) Fe(II) center in PSII (*31*) that results in severe broadening of the EPR signal of Q_A^- (*32*). The Q_A^- semiquinone can be magnetically uncoupled from the Fe(II) center by converting it from the high-spin form (electron spin $S = 2$) to the low-spin form (electron spin $S = 0$) by treatment with CN^- ions (*18*, *33*). In this study, we treat Mn-depleted PSII with CN^- ions to uncouple the Q_A^- semiquinone from the Fe(II) center. As shown in the field sweep electron spin echo spectrum and the derivative EPR line shape in panels A and B of Figure 1, respectively, this facilitates the observation of a narrow $g \sim 2$ EPR signal that is attributed to the uncoupled Q_A^- state of Mn-depleted, CN-treated PSII.

We perform 2D ^{1}H and ^{14}N HYSCORE spectroscopy to probe the magnetic interaction(s) of the paramagnetic Q_A^- state of Mn-depleted, CN-treated PSII. Typically, 2D ^{1}H and ^{14}N HYSCORE spectroscopy measurements yield electron−nuclear hyperfine (and nuclear quadrupolar) coupling parameters that provide valuable information about the electronic and geometric properties of directly bonded nuclei and through-space interactions with nuclei in the vicinity of the electron spin. The hyperfine coupling parameters also provide a measure of the distribution of electron spin density of the paramagnetic species.

The application of ^{1}H and ^{14}N HYSCORE spectroscopy presents several advantages in comparison to previously published one-dimensional (1D) electron nuclear double resonance (ENDOR) and electron spin echo envelope modulation (ESEEM) studies. 2D ^{1}H and ^{14}N HYSCORE spectroscopy dramatically improves the spectral resolution as the addition of a second dimension allows the detection of the hyperfine interactions in a much larger frequency space. This relieves the spectral crowding and overlap that is often observed in ENDOR and 1D ESEEM spectra. In addition, in the case of the electron spin of the Q_A^- semiquinone anion (electron spin $S = {}^1/_2$), the nuclear frequencies are correlated in two dimensions, which significantly simplifies the analysis and assignment of the hyperfine interactions in a 2D ^{1}H and ^{14}N HYSCORE experiment. This allows for the unambiguous interpretation of the experimental spectra.

The 2D HYSCORE spectra of the Q_A^- state in Mn-depleted, CN-treated PSII shown in Figures 1S and 2S of the Supporting Information reveal distinct spectral contributions from the ^{1}H and ^{14}N nuclei that are magnetically interacting with the primary semiquinone state, Q_A^-, of PSII. As one can see in Figures 1S and 2S, the electron−nuclear interactions of Q_A^- with the ^{1}H and ^{14}N nuclei give rise to cross-peaks or ridges that are located near the Zeeman frequency of the corresponding nucleus (ν_{Zeeman}, ^{14}N = 1.06 MHz, and ν_{Zeeman}, ^{1}H = 14.72 MHz) and symmetric with respect to the main diagonal.

Shown in Figure 2A is the expanded region of the (+, +) quadrant of the experimental 2D HYSCORE spectrum that highlights the ^{1}H hyperfine interactions of the Q_A^- state of Mn-depleted, CN-treated PSII at pH 9.8. In the 2D ^{1}H HYSCORE spectrum of the Q_A^- state at pH 9.8 in Figure 2A, we observe five pairs of distinct cross-peaks or ridges that are centered at approximately the proton Zeeman frequency (ν_{Zeeman}, ^{1}H = 14.72 MHz), and each pair of cross-peaks is symmetric with respect to the diagonal of the spectrum. The ridges are labeled H^I, H^{II}, H^{III}, H^{IV}, and H^V and are attributed to protons that are magnetically interacting with the electron spin of the Q_A^- state. The ridges labeled H^{III}, H^{IV}, and H^V are well separated, while the ridges labeled H^I and H^{II} display partial overlap. Ridge H^{IV} consists of two segments, a pronounced segment and a smaller segment, located on different sides with respect to the diagonal. Ridges H^I−H^V are identified by quantitative analysis of the spectrum and are shown to arise from hyperfine interactions of Q_A^- with different types of protons.

Shown in Figure 2B is the numerical simulation of the experimental 2D ^{1}H HYSCORE spectrum of the Q_A^- state at pH 9.8. As one can see, the spectral simulation accurately reproduces the location of the five pairs of ridges that are observed in the experimental 2D ^{1}H HYSCORE spectrum (labeled H^I−H^V) of the Q_A^- state at pH 9.8 (Figure 2A). The anisotropic (T) and isotropic (a_{iso}) proton hyperfine coupling parameters that are obtained via analysis of the data as previously described (*27*) are listed in Table 1A.

The ^{1}H hyperfine (electron−nuclear) interactions are primarily characterized by two parameters, namely, the isotropic and anisotropic hyperfine components, a_{iso} and T, respectively. These components determine the shape and location of the ridges in the frequency space of the 2D HYSCORE spectrum. Qualitatively, the isotropic component corresponds to the average separation of the two ridges in the pair, which is symmetric with respect to the diagonal. The anisotropic component causes a shift of the ridges with respect to the antidiagonal, which is the straight line perpendicular to the diagonal and intersects with the diagonal at the proton Zeeman frequency of 14.72 MHz (Figure 2A). The isotropic component can be interpreted as a measure of electron spin density at the magnetic nucleus, providing information about the spin density distribution of the unpaired electron over the semiquinone anion radical. The anisotropic component arises from the through-space dipolar interaction and provides information about the electron−nuclear distance and the relative geometry of the unpaired electron and the magnetic nucleus. Examination of Table 1A reveals that the values of a_{iso} at pH 9.8 for ridges H^I−H^{III} are 4.58, 7.21, and −6.5 MHz, respectively. The presence of strong isotropic hyperfine interaction, a_{iso}, with the protons contributing to H^I−H^{III} suggests that there is significant orbital overlap that leads to the presence of electron spin density on these protons. This indicates that H^I−H^{III} are directly bonded and are intrinsic to the Q_A^- semiquinone state. In this study, H^I−H^{III} are unambiguously assigned to the electron−nuclear hyperfine interaction of the Q_A^- semiquinone state with the methyl, β-methylene, and ring protons, respectively (Figure 3). The hyperfine parameters that are obtained

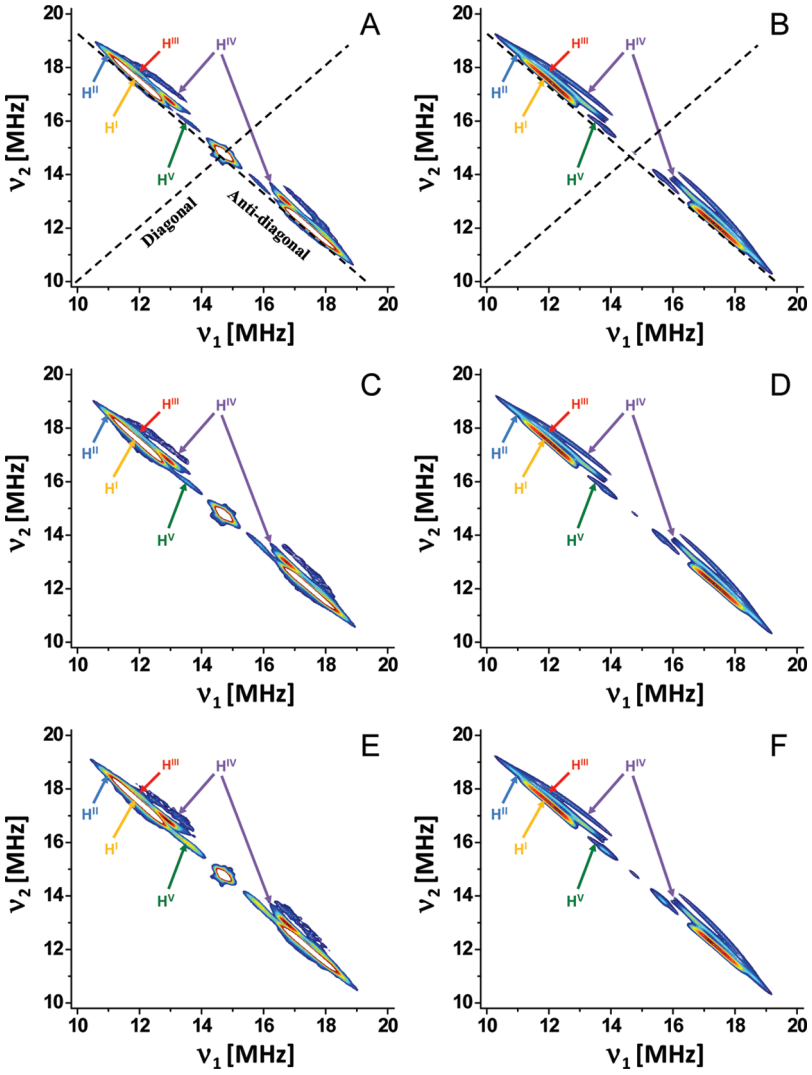

FIGURE 2: (+, +) quadrant of the (A) experimental and (B) simulated 2D ^{1}H HYSCORE spectrum of the Q_A^- semiquinone state of PSII at pH 9.8 with the diagonal and antidiagonal of the spectrum depicted as dashed lines, (C and D) at pH 6.5, and (E and F) at pH 5.5. The labels for the ^{1}H hyperfine ridges are color-coded to match the linear analysis described in the Supporting Information.

here are in excellent agreement with the hyperfine coupling values that were obtained in previous ENDOR spectroscopy studies of the Q_A^- semiquinone state of PSII and plastosemiquinone models in protic solvents (*11*, *27*, *28*, *34*).

As one can see in Figure 2A, the two ridges (labeled H^{IV} and H^V) in the 2D ^{1}H HYSCORE spectrum are shifted from the antidiagonal. Ridge H^{IV} displays a large shift from the antidiagonal, while ridge H^V is less shifted. The values of the anisotropic component (T) of the hyperfine interaction of H^{IV} and H^V at pH 9.8 are 4.66 and 1.78 MHz, respectively (Table 1). The corresponding values of the isotropic component (a_{iso}) of the hyperfine interaction of H^{IV} and H^V at pH 9.8 are −0.27 and −0.19 MHz, respectively. For both H^{IV} and H^V, the value of a_{iso} is significantly smaller than the value of T. The predominantly anisotropic (orientation-dependent) nature of the hyperfine interaction that is reflected in the shift from the antidiagonal and the larger value of T is characteristic of "through-space" dipolar interaction(s) between the unpaired electron spin on the Q_A^- semiquinone and the interacting proton(s). Thus, we assign ridges H^{IV} and H^V as arising from hyperfine interactions of Q_A^- with H-bonded protons of the surrounding protein environment.

There is a difference in the magnitude of the shift from the antidiagonal for ridges H^{IV} and H^V. The larger shift of a ridge from the antidiagonal indicates the presence of a higher anisotropic hyperfine coupling constant (T) and hence a stronger H-bond. This difference in the magnitude of T could arise from a change in either the distance between the hydrogen and carbonyl keto oxygen atom and/or the orientation of the H-bond donor with respect to the plane of the semiquinone ring. Assuming a spin density of 0.25 on the carbonyl oxygen of Q_A^- (*35*) and using a point-dipole approximation for the electron−nuclear dipolar interaction, we estimate the distances between the carbonyl keto oxygen atom of the Q_A^- semiquinone and the H-bonded proton(s) corresponding to ridges H^{IV} and H^V to be 1.62 and 2.23 Å, respectively. This suggests that the H-bond corresponding to H^{IV} is stronger than the H-bond attributed to H^V. However, note that the sign of the isotropic component, a_{iso}, of the hyperfine interaction is sensitive to the orientation of the H-bond. Numerical calculations have previously suggested that the increasing nonplanarity of a H-bond results in a change in the sign of a_{iso} (*29*). Thus, on the basis of the negative a_{iso} values of the H-bond associated with H^{IV} and H^V that are observed in this study (Table 1A), we conclude that both the H-bonds are significantly out of plane relative to the plane of the Q_A^- semiquinone anion. The absolute value of the ratio of a_{iso} to T is ~2 times larger for H^V, which reflects the greater nonplanarity of the H-bond geometry.

Table 1: Hyperfine Coupling Parameters Obtained from the Analysis of the 2D ^{1}H HYSCORE Spectrum at (A) pH 9.8, (B) pH 6.5, and (C) pH 5.5

proton ridge	T (MHz)	a_{iso} (MHz)	$A_\perp$, $A_\parallel$ (MHz)
		(A)	
H^I	1.23 ± 0.1	4.58 ± 0.1	3.35 ± 0.1, 7.03 ± 0.1
H^{II}	1.49 ± 0.2	7.21 ± 0.2	5.73 ± 0.2, 10.2 ± 0.2
H^{III}	2.89 ± 0.4	−6.5 ± 0.4	−9.38 ± 0.4, −0.75 ± 0.4
H^{IV}	4.66 ± 0.05	−0.27 ± 0.05	−4.92 ± 0.05, 9.05 ± 0.05
H^V	1.78 ± 0.2	−0.19 ± 0.2	−1.96 ± 0.2, 3.37 ± 0.2
		(B)	
H^I	1.25 ± 0.1	4.71 ± 0.1	3.46 ± 0.1, 7.22 ± 0.1
H^{II}	1.44 ± 0.2	7.19 ± 0.2	5.75 ± 0.2, 10.09 ± 0.2
H^{III}	2.86 ± 0.4	−6.39 ± 0.4	−9.25 ± 0.4, −0.68 ± 0.4
H^{IV}	4.77 ± 0.1	−0.27 ± 0.1	−5.03 ± 0.1, 9.27 ± 0.1
H^V	1.82 ± 0.2	−0.31 ± 0.2	−2.13 ± 0.2, 3.34 ± 0.2
		(C)	
H^I	1.19 ± 0.1	4.79 ± 0.1	3.59 ± 0.1, 7.18 ± 0.1
H^{II}	1.45 ± 0.2	7.03 ± 0.2	5.58 ± 0.2, 9.92 ± 0.2
H^{III}	2.83 ± 0.4	−6.36 ± 0.4	−9.20 ± 0.4, −0.69 ± 0.4
H^{IV}	4.72 ± 0.6	−0.39 ± 0.6	−5.10 ± 0.6, 9.05 ± 0.6
H^V	1.83 ± 0.2	−0.41 ± 0.2	−2.24 ± 0.2, 3.25 ± 0.2

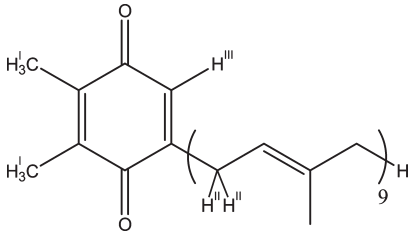

FIGURE 3: Structure of a plastoquinone molecule. Highlighted are the methyl (H^I), β-methylene (H^{II}), and ring (H^{III}) protons that are observed in the 2D ^{1}H HYSCORE spectra shown in Figure 2.

To assign the putative H-bond partners, we perform 2D ^{14}N HYSCORE spectroscopy on the Q_A^- state of Mn-depleted CN-treated PSII. Figure 4A depicts the expanded region of the (+, +) quadrant of the experimental 2D HYSCORE spectrum of the Q_A^- state of Mn-depleted, CN-treated PSII at pH 9.8 (Figure 1S of the Supporting Information), which highlights the interactions with the surrounding ^{14}N nuclei. In the 2D ^{14}N HYSCORE experimental spectrum shown in Figure 4A, there are two pairs of ridges located in the low-frequency region near double the ^{14}N Zeeman frequency that are symmetric with respect to the diagonal with maximal signal intensity at [(2.86 MHz, 5.01 MHz), (5.01 MHz, 2.86 MHz)] and [(1.69 MHz, 3.96 MHz), (3.96 MHz, 1.69 MHz)], respectively. The values of the three principal hyperfine components, a_{iso}, the nuclear quadrupole coupling constant, K, and the asymmetry parameter of the nuclear quadrupole tensor, η, were obtained from comparison of the experimental (Figure 4A) and simulated (Figure 4B) spectra, and the values are listed in Table 2A.

In contrast to the magnetic nature of the electron−nuclear hyperfine tensor, the quadrupole interaction is determined by electric field gradients that are experienced by the nucleus when the nuclear spin $I > {}^1/_2$. The quadrupole tensor parameters K and η reflect the size and asymmetry of the electric field gradient at the position of the nucleus. These parameters are determined by the local electronic structure around the nucleus and can be used to identify the type of chemical bonding of the nucleus. The quadrupole coupling constant, K, and the asymmetry parameter, η, of N^I at pH 9.8 that were obtained in this study are characteristic of nuclear quadrupole interaction of an amide nitrogen of the peptide backbone. The value of K observed here is in good agreement with previously published values for a peptide nitrogen in polyglycine (*36*). The values of K and η of N^{II} at pH 9.8 that are obtained here are typical of a nuclear quadrupole interaction with an amino nitrogen of the imidazole side chain of a His residue (*37*). The large a_{iso} value that is observed for both N^I and N^{II} indicates the presence of significant electron spin density on the nitrogen atoms. This requires the presence of an atomic bridge that would allow for electron spin density to be transferred from Q_A^- to the nitrogen atom(s) of the amino acid residue(s). This is attributed to the presence of strong H-bonding interactions between the Q_A^- semiquinone and the nitrogen atoms, N^I and N^{II}.

In this study, we also examine the effect of pH on the H-bonded protons, the backbone peptide and amino nitrogen atoms that serve as H-bond donors to the Q_A^- semiquinone state. In addition to examining the Q_A^- state of Mn-depleted, CN-treated PSII at pH 9.8, we examine the 2D ^{1}H and ^{14}N HYSCORE spectra of the Q_A^- state at pH 6.5 and 5.5, respectively. Shown in panels C and E of Figure 2 are the experimental 2D ^{1}H HYSCORE spectra of the Q_A^- state at pH 6.5 and 5.5, respectively. The corresponding values of the isotropic (a_{iso}) and anisotropic (T) components of the hyperfine interaction that were obtained from the linear analysis (described in Materials and Methods) are listed in parts B and C of Table 1 for pH 6.5 and 5.5, respectively. The numerical simulations of the experimental spectra using the parameters that were obtained from the linear analysis are shown in panels D and F of Figure 2. As one can see in Table 1A−C, both isotropic (a_{iso}) and anisotropic (T) components of the hyperfine interaction for H^{IV} and H^V remain unchanged within the estimated experimental error. This indicates that although subtle changes in either the geometry or the distance of the bonds might be masked by experimental inaccuracy, there is no significant change in the strength, planarity, or orientation of the H-bond with the change in pH (*29*).

The experimental and simulated ^{14}N HYSCORE spectra of the Q_A^- state of PSII at pH 6.5 and 5.5 are shown in panels C and D of Figure 4 and panels E and F of Figure 4, respectively. At pH 6.5, the ridges have maximal signal intensity at [(2.86 MHz, 5.05 MHz), (5.05 MHz, 2.86 MHz)] and [(1.63 MHz, 4.1 MHz), (4.1 MHz, 1.63 MHz)], respectively, and at pH 5.5, they have maximal signal intensity at [(2.89 MHz, 4.89 MHz), (4.89 MHz, 2.89 MHz)] and [(1.53 MHz, 4.14 MHz), (4.14 MHz, 1.53 MHz)], respectively. The electron−nuclear hyperfine and the nuclear quadrupole parameters are obtained from comparison of the experimental (Figure 4C,E) and corresponding simulated spectra (Figure 4D,F), and these are listed in Table 2B. While the nuclear quadrupole coupling constant, K, and the asymmetry parameter, η, are virtually identical at pH 9.8, 6.5, and 5.5, we observe a small variation of the principal components of the electron−nuclear hyperfine tensor for both N^I and N^{II}. However, the observed variations are within the estimated error and the reproducibility of the experiment. This observation is in agreement with the absence of a pH dependence of the 2D ^{1}H spectra that are very sensitive to even small perturbations of the H-bonding interactions. Thus, neither ^{1}H nor ^{14}N spectra demonstrate a dependence of the hydrogen bond strength and geometry on the pH of the PSII sample. This is in contrast to previously published literature that reports the presence of effects of pH on the H-bond with N^{II} (*9*, *38*). However, our results compare well with previous

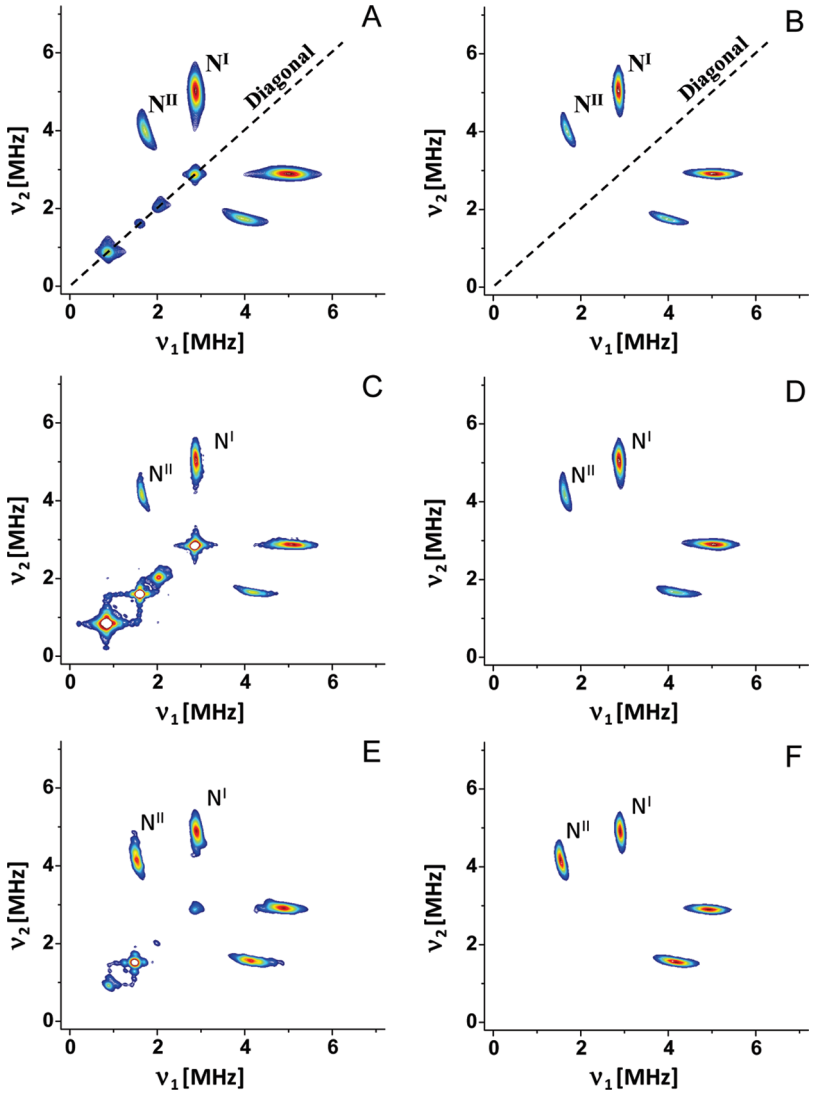

FIGURE 4: (+, +) quadrant of the (A) experimental and (B) simulated 2D ^{14}N HYSCORE spectrum of the Q_A^- semiquinone state of PSII at pH 9.8, (C and D) at pH 6.5, and (E and F) at pH 5.5.

Table 2: Hyperfine Coupling Parameters Obtained from the Analysis of the 2D ^{14}N HYSCORE Spectrum at (A) pH 9.8, (B) pH 6.5, and (C) pH 5.5

nitrogen ridge	A_x, A_y, A_z (MHz)[a]	a_{iso} (MHz)	α, β, γ (deg)[b]	K (MHz)	η
		(A)			
N^I	2.2, 1.1, 2.4 (±0.2)	1.9 ± 0.2	0, 45, 0	0.81 ± 0.02	0.46 ± 0.1
N^{II}	1.8, 1.0, 1.2 (±0.2)	1.3 ± 0.2	0, 0, 0	0.40 ± 0.02	0.85 ± 0.1
		(B)			
N^I	2.1, 1.0, 2.3 (±0.2)	1.8 ± 0.2	0, 45, 0	0.81 ± 0.02	0.47 ± 0.1
N^{II}	2.0, 1.2, 1.4 (±0.2)	1.5 ± 0.2	0, 0, 0	0.40 ± 0.02	0.83 ± 0.1
		(C)			
N^I	1.9, 1.0, 2.1 (±0.2)	1.7 ± 0.2	0, 45, 0	0.82 ± 0.02	0.47 ± 0.1
N^{II}	2.0, 1.2, 1.4 (±0.2)	1.5 ± 0.2	0, 0, 0	0.38 ± 0.02	0.82 ± 0.1

[a]Deviation applies to each value. [b]Euler angles of the quadrupole tensor in the principal axis frame of the hyperfine tensors.

ESEEM investigations on Zn-substituted PSII and high-pH treated PSII (*9*, *10*, *13*).

DISCUSSION

We demonstrate the simultaneous application of 2D ^{1}H and ^{14}N HYSCORE spectroscopy to characterize the H-bond interactions of the reduced Q_A^- state of Mn-depleted, CN-treated PSII with the surrounding amino acid residues of the protein matrix. The application of 2D HYSCORE spectroscopy renders several advantages over conventional 1D EPR spectroscopy methods, such as ENDOR and 1D ESEEM spectroscopy, which are used to detect electron−nuclear hyperfine couplings. In the

2D HYSCORE experiment, the electron−nuclear hyperfine interactions are detected in a much larger frequency space that provides superior resolution. The 2D HYSCORE experiment provides a more accurate measure of through-space highly anisotropic hyperfine couplings that are a signature of H-bond interactions. Further, in this study, we combine the interpretation of the strength and geometry of H-bonds using 2D ^{1}H HYSCORE spectroscopy with the assignment of the H-bond donors by ^{14}N HYSCORE spectroscopy.

In the 2D ^{1}H HYSCORE spectrum of the Q_A^- state of Mn-depleted, CN-treated PSII at pH 9.8, we detect five different types of protons (contributing to the cross-peaks or ridges H^I−H^V) that are interacting with the semiquinone anion (Figure 2A and Figures 3S and 4S of the Supporting Information). On the basis of the hyperfine parameters that were obtained here (Table 1A) and comparison with previously published data (*11*, *27*, *28*, *34*), we assign ridges H^I−H^{III} as arising from the hyperfine interaction of the Q_A^- state with intrinsic protons, namely, the methyl, β-methylene, and ring protons, respectively (Figure 3). In addition, we observe two ridges, H^{IV} and H^V (Figure 2A), that are due to predominant anisotropic electron−nuclear hyperfine couplings (Table 1A). This is characteristic of "through-space" orientation-dependent dipolar interaction(s) between the unpaired electron spin on the semiquinone and the interacting proton(s). Thus, we assign the ridges, H^{IV} and H^V, as arising from hyperfine interactions of the Q_A^- semiquinone with H-bonded protons of the surrounding protein matrix.

As one can see in Table 1A, there is a difference in the magnitude of the anisotropic hyperfine coupling, T, for ridges H^{IV} and H^V. This indicates a difference in the strength of the respective H-bonds. On the basis of the larger anisotropic hyperfine coupling, T, of H^{IV} in comparison with H^V, we conclude that the H-bond corresponding to H^{IV} is significantly stronger than the H-bond attributed to H^V. This difference is largely due to a difference in the H-bond length, i.e., the distance between the carbonyl keto oxygen atom of the Q_A^- semiquinone and the H-bonded proton. The sign of the isotropic component, a_{iso}, of the hyperfine interaction and its relative size with respect to T are sensitive to the orientation of the H-bond (*29*). The negative sign of a_{iso} of both H^{IV} and H^V in Table 1A indicates that the H-bonds are twisted out of the plane of the ring of the Q_A^- semiquinone. The relative size of the isotropic hyperfine component, a_{iso}, with respect to T is observed to be larger for ridge H^V, which indicates the stronger nonplanarity of the H-bond geometry.

We determine the perpendicular and parallel components of the hyperfine tensor, $A_\perp$ and $A_\parallel$, respectively, of the H-bonded protons that contribute to ridges H^{IV} and H^V of the 2D ^{1}H HYSCORE spectrum of the Q_A^- state of Mn-depleted, CN-treated PSII at pH 9.8 (Table 1A). At pH 6.5, the hyperfine components ($A_\perp$ and $A_\parallel$) were estimated by ^{1}H ENDOR to be 4.8 and −1.1 MHz, respectively, for the first H-bond and −2.2 and 4.4 MHz, respectively, for the second hydrogen bond (*11*). In this ENDOR study, the authors attribute the first interaction to an asymmetric weak H-bond and the second interaction to a stronger H-bond that was similar to the H-bond of the plasto-semiquinone radical in a frozen solution of isopropyl alcohol. The H-bonds were not assigned to specific amino acid residues in the protein matrix. In our study, $A_\perp$ and $A_\parallel$ for the H-bonded proton of ridge H^{IV} at pH 6.5 were determined to be −5.03 and 9.27 MHz, respectively, which are not in agreement with the values obtained for the first H-bonded proton in the ^{1}H ENDOR study (*11*). However, the $A_\perp$ and $A_\parallel$ values of the second H-bonded proton (ridge H^V), 2.13 and 3.34 MHz, respectively, are in reasonable agreement with the second H-bonded proton (*11*). This discrepancy between the two studies could be attributed to the difference in spectral resolution between the previous ^{1}H ENDOR (*11*) and present HYSCORE spectroscopy study. HYSCORE spectroscopy is a superior tool for the detection of electron−nuclear hyperfine interactions that are predominantly dipolar in nature, while such interactions often remain poorly resolved in ENDOR spectra.

To identify the donors that participate in the H-bonding interactions of the reduced Q_A^- state of PSII, we study the nuclear quadrupole and the electron−nuclear ^{14}N hyperfine couplings using 2D ^{14}N HYSCORE spectroscopy. The quadrupolar interaction provides insight into the type of ^{14}N nucleus that is interacting with the Q_A^- state. In the study of the Q_A^- state at pH 9.8, the values of asymmetry parameter, η, and the quadrupolar coupling constant, K, of the two nitrogen atoms, N^I and N^{II}, are assigned to a peptide backbone nitrogen and an amino nitrogen of a His residue, respectively (Table 2A). These assignments are in agreement with those from previously published studies by Rutherford (*9*, *38*), Astashkin (*13*), and co-workers (Table 3).

Examination of the X-ray crystal structures of PSII (*2*, *3*, *5*) reveals the presence of two nitrogen atoms that could interact with the Q_A^- semiquinone through H-bonding interactions. There is an amide nitrogen atom of the peptide backbone (D2-Phe261) and an amino nitrogen atom of an imidazole side chain (D2-His214) in the protein matrix that are in the proximity of the neutral Q_A center in the X-ray structure of PSII (Figure 5A). On the basis of the quadrupole coupling parameters listed in Table 2A, ridges N^I and N^{II} in the 2D ^{14}N HYSCORE spectrum could be attributed to the electron−nuclear hyperfine interactions of the reduced Q_A^- state with the amide and the amino nitrogen atom of D2-Phe261 and D2-His214, respectively. However, it is important to note that X-ray crystal structures of PSII depict the environment of the neutral primary quinone, Q_A, whereas its reduced semiquinone state, Q_A^-, is observed by EPR spectroscopy. It is plausible that the strength and symmetry of the H-bonds are significantly different between the neutral Q_A and reduced Q_A^- semiquinone state, respectively.

It is important to mention that specific isotope labeling and site-directed mutagenesis studies of PSII performed by Peloquin et al. (*15*) have previously suggested a very weak interaction between the amide peptide nitrogen of D2-Ala260 and the Q_A^- state. The authors observed a single amide peptide nitrogen nucleus with hyperfine parameters close to the values obtained for N^I in this study. By comparing the values of the isotropic hyperfine coupling, a_{iso}, that are obtained for nitrogen atoms N^I and N^{II} in our 2D ^{14}N HYSCORE study, we confirm the presence of highly asymmetric H-bonds in the reduced Q_A^- semiquinone state. The significantly larger a_{iso} value for N^I indicates a higher spin density at the peptide nitrogen atom. This reflects a stronger H-bonding interaction between the carbonyl oxygen atom of the Q_A^- semiquinone and the corresponding peptide bond compared to that of the interaction previously estimated in the literature (*15*). This further confirms that proton H^{IV} can likely be assigned to D2-Phe261 and H^V to D2-His214.

In this study, we explore the pH dependence of the H-bonding interactions of the reduced Q_A^- semiquinone state. On the basis of the estimated pK_a value of an amide peptide group, we do not expect a pH dependence of the 2D ^{1}H and ^{14}N HYSCORE signals of the H-bond to the amide peptide backbone group at pH values ranging from 9.8 to 5.5. The value of the electron−nuclear hyperfine parameters, a_{iso} and T, of N^I remain unchanged at

Table 3: Comparison of ^{14}N Hyperfine Coupling Parameters Obtained in This Study with Those from Previously Published Reports

	nitrogen cross-peak (N^I)			nitrogen cross-peak (N^{II})		
	A_x, A_y, A_z (MHz)	K (MHz)	η	A_x, A_y, A_z (MHz)	K (MHz)	η
Mn-depleted, CN-treated PSII (pH 9.8)[a]	2.2, 1.1, 2.4	0.81	0.46	1.8, 1.0, 1.2	0.40	0.85
CN-treated PSII (pH 9.2)[b]	2.0, 1.7, 2.6	0.8125	0.45	0.2, 0.2, 0.9	0.4125	0.75
CN-treated PSII (pH 8.2)[b]	2.0, 1.7, 2.6	0.8125	0.45	1.1, 1.1, 1.9	0.4125	0.75
Zn-substituted PSII (pH 8.8)[c]	1.9	0.75−0.85	0.40−0.77	1.9	0.32−0.37	0.88−0.97

[a]This work. [b]From ref *9*. [c]From ref *13*.

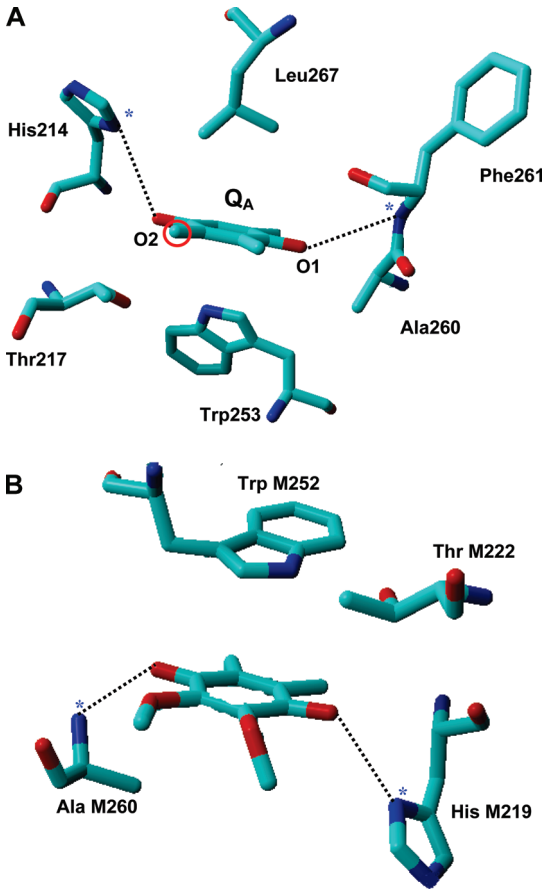

FIGURE 5: (A) Structure of the binding site of the primary quinone, Q_A, as seen in the X-ray crystal structure of PSII (*2*, *3*, *5*). Shown are the amino acid residues that are suggested to be involved in H-bonding, hydrophobic, and π-stacking interactions in the Q_A-binding site of PSII (the phytyl tail of Q_A has been omitted for the sake of clarity). Highlighted are the magnetically interacting nitrogen atoms (asterisks), the carbon atom of the bulky methyl group (red circle), and the hydrogen bonds (dashed lines) that are detected in this study of the Q_A^- semiquinone of PSII (Protein Data Bank entry 1S5L). (B) Structure of the binding site of the primary quinone, Q_A, as seen in the X-ray crystal structure of BRC (*44*). Shown are the amino acid residues that are suggested to be involved in H-bonding, hydrophobic, and π-stacking interactions in the Q_A-binding site of BRC (the phytyl tail of Q_A has been omitted for the sake of clarity). Highlighted are the magnetically interacting nitrogen atoms (asterisk) and the hydrogen bonds (dashed lines) that were previously detected in ENDOR studies of the Q_A^- semiquinone of the BRC (Protein Data Bank entry 1PCR).

pH 9.8, 6.5, and 5.5 (Tables 1 and 2). This is in agreement with previous results for CN-treated PSII, Zn-substituted PSII, and high-pH-treated PSII (Table 3) (*9*, *13*, *14*, *38*).

In this study, we also investigate the pH dependence of the H-bonding interaction of the Q_A^- state with the amino nitrogen of the imidazole side chain of the His residue (N^{II}) (Table 2). We do not observe a dependence of N^{II} on pH values ranging from 9.8 to 5.5; there is a slight variation in the electron−nuclear hyperfine couplings, but this is within experimental error. There are contrasting reports about the pH dependence of the N^{II} atom of the amino nitrogen atom of the imidazole side chain in the literature (*9*, *38*). In a study performed by Rutherford and coworkers (*9*), the authors observed a pH dependence of the H-bond strength of the amino group of an imidazole side chain. It was observed that in CN-treated PSII, an increase in the pH results in a decrease in the electron−nuclear hyperfine couplings of the N^{II} atom leading to the almost complete disappearance of the H-bond at pH >9. However, such a pH dependence was not observed in previous studies of high-pH-treated PSII (Table 3). The absence of this pH dependence was also confirmed by a detailed study of Zn-substituted PSII (*13*). In the latter studies, the authors attribute the previous observation of the deprotonation of the amino group of the imidazole at high pH to the biochemical treatment used to uncouple the iron. In this study, the ^{14}N HYSCORE spectra of the Q_A^- semiquinone of Mn-depleted, CN-treated PSII are compared with the corresponding spectra of Fe(II)Q_A^- in intact PSII to ensure the structural integrity of the treated PSII samples.

It is well-known that the estimated pK_a value of an imino group of an uncoordinated His residue is ~6.0. However, in the case of a His residue coordinated to the non-heme iron of PSII, the imino group is deprotonated at a lower pH value. This seems to be in agreement with the observed deprotonation in the CN-treated PSII sample in previous studies (*9*). In the case of a metal-coordinated His residue, the second deprotonation of imidazole (amino group) is improbable at pH $\leq$10.0. This is supported by the results of Sorkin et al. (*39*), who observed an iron-coordinated His residue in the protonated form in iron-superoxide dismutase using NMR spectroscopy. This is in agreement with the absence of a pH dependence in our study.

There are structural similarities among the type II RCs, PSII, and the reaction center from purple bacteria (BRC) (*2*, *40*). Although the quinone that is recruited in the Q_A site is different in the two RCs (plastoquinone and ubiquinone in PSII and the BRC, respectively), there are significant similarities between PSII and BRC that extend to the molecular interactions of the binding site of the primary quinone, Q_A, and the estimated midpoint potentials of Q_A in PSII and the BRC (approximately −148 and −180 mV in PSII and the BRC, respectively) (*41*, *42*). Previous ENDOR spectroscopy studies of the Q_A^- state of the BRC have suggested the presence of two H-bonds that are nearly equivalent in strength (*43*) (Table 4). The hyperfine parameters for the interaction of Q_A^- of PSII with the H-bonded proton that contributes to ridge H^{IV} (Table 4) are almost identical to the hyperfine parameters reported for the H-bond with AlaM260 in the BRC (Table 4). However, the second H-bond of Q_A^- of PSII, H^V,

Table 4: Comparison of ^{1}H Hyperfine Coupling Parameters Obtained in This Study with Those from Previously Published Reports

	anisotropic hyperfine coupling constants ($A_\parallel$, $A_\perp$) (MHz)	proton assignment
PSII, Q_A^{-a}	9.05, −4.92	H^{IV}
	3.37, −1.96	H^{V}
BRC, Q_A^{-b}	8.95, −4.93	AlaM260
	9.15, −6.51	HisM219

[a]This work. Data obtained at pH 9.8. [b]From ref *43*.

is weaker than the H-bond with HisM219 (Table 4). This difference could be due to structural differences in the protein environment in PSII and BRC as well as a difference in the substituent groups of plastoquinone and ubiquinone. For the H-bond with D2-His214 of PSII, the presence of a negative isotropic component of the proton hyperfine interaction suggests the presence of a nonplanar H-bond. This nonplanarity can be observed in the crystallographic data (see Figure 5A) in which the angle between the amino nitrogen of D2-His214 and the C−O bond of the carbonyl group is ∼56°. This could be due to the presence of bulky methyl group substituents on the primary quinone that are ∼4.95 Å from the D2-His214 residue, which is likely to cause steric hindrance that places the D2-His214 residue outside of the quinone ring plane (Figure 5A). In contrast, less nonplanarity is observed in the crystal structure of BRC where the angle between the amino nitrogen of HisM219 and the C−O bond of the carbonyl group is ∼41° (*44*) (Figure 5B). Similar to our observation for the D2-His214 residue of PSII, highly nonplanar hydrogen bonds were detected for the ubiquinone, Q_i, of the cytochrome bc_1 complex (*23*), where the nonplanarity results in the presence of a significant isotropic component of the hyperfine interaction.

The presence of strong H-bonds is expected to stabilize the Q_A^- semiquinone of PSII (*1*) as these interactions drive the midpoint potential to a higher (more positive) value. While it is not possible to account for the large midpoint potential of the Q_A acceptor of PSII solely on the basis of the differences in the strength and relative orientation of H-bonds, H-bonding patterns are an important determinant of the redox properties of quinone function in PSII. The difference in the H-bonding patterns between the two quinone acceptors, Q_A and Q_B, of PSII could be one of the factors contributing to the difference in their redox potentials (*42*) (approximately −148 and −62 mV, respectively) and function. Also, it is known for the BRC that a change in pH leads to a change in the rate of transfer of an electron from Q_A^- to Q_B. It is proposed for the BRC that the electron transfer rate is gated by pH-dependent conformational changes (*45*). Because there are remarkable similarities between the BRC and PSII, similar pH-dependent conformational changes are expected in PSII. However, we do not observe a significant pH dependence of the H-bonding pattern of Q_A^- in PSII, implying that such conformational changes would not involve a change in the H-bonding patterns of Q_A^- in PSII.

In this study, for the first time, we demonstrate the application of 2D ^{1}H HYSCORE spectroscopy in resolving the individual asymmetric H-bonds of the primary quinone acceptor of PSII and obtain quantitative information about the strength and orientation of the H-bonds to the bound cofactor in the semiquinone state. This is significant as it provides direct insight into the redox tuning of the primary quinone of PSII and facilitates direct comparison of the Q_A site of PSII with the quinone-binding sites of the BRC, PSI, and the cytochrome bc_1 complex.

SUPPORTING INFORMATION AVAILABLE

Field sweep electron spin echo spectra, four-pulse and six-pulse HYSCORE spectra, and details of the linear analysis of the proton hyperfine interactions of the Q_A^- state of PSII. This material is available free of charge via the Internet at http://pubs.acs.org.

REFERENCES

1. Srinivasan, N., and Golbeck, J. H. (2009) Protein-cofactor interactions in bioenergetic complexes: The role of the A_{1A} and A_{1B} phylloquinones in Photosystem I. *Biochim. Biophys. Acta 1787*, 1057–1088.
2. Guskov, A., Kern, J., Gabdulkhakov, A., Broser, M., Zouni, A., and Saenger, W. (2009) Cyanobacterial photosystem II at 2.9 angstrom resolution and the role of quinones, lipids, channels and chloride. *Nat. Struct. Mol. Biol. 16*, 334–342.
3. Ferreira, K. N., Iverson, T. M., Maghlaoui, K., Barber, J., and Iwata, S. (2004) Architecture of the photosynthetic oxygen-evolving center. *Science 303*, 1831–1838.
4. Debus, R. J., Feher, G., and Okamura, M. Y. (1986) Iron-depleted reaction centers from *Rhodopseudomonas sphaeroides* R-26.1: Characterization and reconstitution with Fe^{2+}, Mn^{2+}, Co^{2+}, Ni^{2+}, Cu^{2+}, and Zn^{2+}. *Biochemistry 25*, 2276–2287.
5. Loll, B., Kern, J., Saenger, W., Zouni, A., and Biesiadka, J. (2005) Towards complete cofactor arrangement in the 3.0 angstrom resolution structure of photosystem II. *Nature 438*, 1040–1044.
6. Kamiya, N., and Shen, J. R. (2003) Crystal structure of oxygen-evolving photosystem II from *Thermosynechococcus vulcanus* at 3.7 angstrom resolution. *Proc. Natl. Acad. Sci. U.S.A. 100*, 98–103.
7. Zheng, M., and Dismukes, G. C. (1996) The conformation of the isoprenyl chain relative to the semiquinone head in the primary electron acceptor Q_A of higher plant PSII (plastosemiquinone) differs from that in bacterial reaction centers (ubisemiquinone or menasemiquinone) by ca. 90°. *Biochemistry 35*, 8955–8963.
8. Kern, J., and Renger, G. (2007) Photosystem II: Structure and mechanism of the water:plastoquinone oxidoreductase. *Photosynth. Res. 94*, 183–202.
9. Deligiannakis, Y., Hanley, J., and Rutherford, A. W. (1999) 1D- and 2D-ESEEM study of the semiquinone radical Q_A^- of photosystem II. *J. Am. Chem. Soc. 121*, 7653–7664.
10. Deligiannakis, Y., Jegerschold, C., and Rutherford, A. W. (1997) EPR and ESEEM study of the plastoquinone anion radical Q_A^- in photosystem II treated at high pH. *Chem. Phys. Lett. 270*, 564–572.
11. Macmillan, F., Lendzian, F., Renger, G., and Lubitz, W. (1995) EPR and ENDOR investigation of the primary electron-acceptor radical-anion Q_A^- in iron-depleted photosystem II membrane fragments. *Biochemistry 34*, 8144–8156.
12. Deligiannakis, Y., Boussac, A., and Rutherford, A. W. (1995) ESEEM study of the plastoquinone anion radical Q_A^- in N-14- and N-15-labeled photosystem II treated with CN. *Biochemistry 34*, 16030–16038.
13. Astashkin, A. V., Kawamori, A., Kodera, Y., Kuroiwa, S., and Akabori, K. (1995) An electron-spin echo envelope modulation study of the primary acceptor quinone in Zn-substituted plant photosystem II. *J. Chem. Phys. 102*, 5583–5588.
14. Astashkin, A. V., Hara, H., Kuroiwa, S., Kawamori, A., and Akabori, K. (1998) A comparative electron spin echo envelope modulation study of the primary electron acceptor quinone in Zn-substituted and cyanide-treated preparations of photosystem II. *J. Chem. Phys. 108*, 10143–10151.
15. Peloquin, J. M., Tang, X. S., Diner, B. A., and Britt, R. D. (1999) An electron spin-echo envelope modulation (ESEEM) study of the Q_A binding pocket of PS II reaction centers from spinach and *Synechocystis*. *Biochemistry 38*, 2057–2067.
16. Berthold, D. A., Babcock, G. T., and Yocum, C. F. (1981) A highly resolved, oxygen-evolving photosystem-II preparation from spinach thylakoid membranes: Electron paramagnetic resonance and electron transport properties. *FEBS Lett. 134*, 231–234.
17. Tamura, N., and Cheniae, G. (1987) Photoactivation of the water-oxidizing complex in photosystem II membranes depleted of Mn and extrinsic proteins.1. Biochemical and kinetic characterization. *Biochim. Biophys. Acta 890*, 179–194.
18. Deligiannakis, Y., and Rutherford, A. W. (1998) Reaction centre photochemistry in cyanide-treated photosystem II. *Biochim. Biophys. Acta 1365*, 354–362.
19. Milikisiyants, S., Chatterjee, R., Weyers, A., Meenaghan, A., Coates, C., and Lakshmi, K. V. (2010) Ligand environment of the S_2 state of photosystem II: A study of the hyperfine interactions of the tetranuclear manganese cluster by 2D N-14 HYSCORE spectroscopy. *J. Phys. Chem. B 114*, 10905–10911.

20. Hofer, P., Grupp, A., Nebenfuhr, H., and Mehring, M. (1986) Hyperfine sublevel correlation (HYSCORE) spectroscopy: A 2D electron-spin-resonance investigation of the squaric acid radical. *Chem. Phys. Lett. 132*, 279–282.
21. Schweiger, A., and Jeschke, G. (2001) Principles of pulse electron paramagnetic resonance, p 288, Oxford University Press, Oxford, U.K.
22. Kasumaj, B., and Stoll, S. (2008) 5-and 6-pulse electron spin echo envelope modulation (ESEEM) of multi-nuclear spin systems. *J. Magn. Reson. 190*, 233–247.
23. Song, R., Zhong, Y. C., Noble, C. J., Pilbrow, J. R., and Hutton, D. R. (1995) A new 6-pulse 2-dimensional electron-spin echo envelope modulation (ESEEM) correlation spectroscopy. *Chem. Phys. Lett. 237*, 86–90.
24. Stoll, S., Calle, C., Mitrikas, G., and Schweiger, A. (2005) Peak suppression in ESEEM spectra of multinuclear spin systems. *J. Magn. Reson. 177*, 93–101.
25. Dikanov, S. A., and Bowman, M. K. (1995) Cross-peak lineshape of 2-dimensional ESEEM spectra in disordered $S = 1/2$, $I = 1/2$ spin systems. *J. Magn. Reson., Ser. A 116*, 125–128.
26. Dikanov, S. A., Samoilova, R. I., Kolling, D. R. J., Holland, J. T., and Crofts, A. R. (2004) Hydrogen bonds involved in binding the Q_i-site semiquinone in the bc_1 complex, identified through deuterium exchange using pulsed EPR. *J. Biol. Chem. 279*, 15814–15823.
27. Weyers, A. M., Chatterjee, R., Milikisiyants, S., and Lakshmi, K. V. (2009) Structure and function of quinones in biological solar energy transduction: A differential pulse voltammetry, EPR, and hyperfine sublevel correlation (HYSCORE) spectroscopy study of model benzoquinones. *J. Phys. Chem. B 113*, 15409–15418.
28. Burghaus, O., Plato, M., Rohrer, M., Mobius, K., Macmillan, F., and Lubitz, W. (1993) 3-mm high-field EPR on semiquinone radical-anions $Q^{\bullet-}$ related to photosynthesis and on the primary donor $P^{\bullet+}$ and acceptor $Q_A^{\bullet-}$ in reaction centers of *Rhodobacter sphaeroides* R-26. *J. Phys. Chem. 97*, 7639–7647.
29. O'Malley, P. J. (1998) A density functional study of the effect of orientation of hydrogen bond donation on the hyperfine couplings of benzosemiquinones: Relevance to semiquinone-protein hydrogen bonding interactions in vivo. *Chem. Phys. Lett. 291*, 367–374.
30. Stoll, S., and Schweiger, A. (2006) EasySpin, a comprehensive software package for spectral simulation and analysis in EPR. *J. Magn. Reson. 178*, 42–55.
31. Rutherford, A. W., and Zimmermann, J. L. (1984) A new electron paramagnetic resonance signal attributed to the primary plastoquinone acceptor in photosystem II. *Biochim. Biophys. Acta 767*, 168–175.
32. Miller, A. F., and Brudvig, G. W. (1991) A guide to electron paramagnetic resonance spectroscopy of photosystem II membranes. *Biochim. Biophys. Acta 1056*, 1–18.
33. Sanakis, Y., Petrouleas, V., and Diner, B. A. (1994) Cyanide binding at the non-heme Fe^{2+} of the iron-quinone complex of photosystem II: At high concentrations, cyanide converts the Fe^{2+} from high ($S = 2$) to low ($S = 0$) spin. *Biochemistry 33*, 9922–9928.
34. MacMillan, F., Lendzian, F., and Lubitz, W. (1995) EPR and ENDOR characterization of semiquinone anion radicals related to photosynthesis. *Magn. Reson. Chem. 33*, S81–S93.
35. Himo, F., Babcock, G. T., and Eriksson, L. A. (1999) Conformational analysis of quinone anion radicals in photosystem II and photosynthetic bacteria. *J. Phys. Chem. A 103*, 3745–3749.
36. Blinc, R., Mali, M., Osredkar, R., Seliger, J., and Ehrenber, L. (1974) N-14 quadrupole resonance in polyglycine. *Chem. Phys. Lett. 28*, 158–159.
37. Edmonds, D. T. (1977) Nuclear-quadrupole double-resonance. *Phys. Rep. 29*, 234–290.
38. Deligiannakis, Y., and Rutherford, A. W. (2000) Effect of pH on the semiquinone radical Q_A^- in CN-treated photosystem II: Study by hyperfine sublevel correlation spectroscopy. *J. Inorg. Biochem. 79*, 339–345.
39. Sorkin, D. L., and Miller, A. F. (1997) Spectroscopic measurement of a long-predicted active site pK in iron-superoxide dismutase from *Escherichia coli*. *Biochemistry 36*, 4916–4924.
40. Deisenhofer, J., Epp, O., Miki, K., Huber, R., and Michel, H. (1985) Structure of the protein subunits in the photosynthetic reaction center of *Rhodopseudomonas viridus* at 3 Å resolution. *Nature 318*, 618–624.
41. Arata, H., and Parson, W. W. (1981) Delayed fluorescence from *Rhodopseudomonas sphaeroides* reaction centers: Enthalpy and free energy changes accompanying electron-transfer from P_{870} to quinones. *Biochim. Biophys. Acta 638*, 201–209.
42. Ishikita, H., and Knapp, E. W. (2005) Control of quinone redox potentials in photosystem II: Electron transfer and photoprotection. *J. Am. Chem. Soc. 127*, 14714–14720.
43. Flores, M., Isaacson, R., Abresch, E., Calvo, R., Lubitz, W., and Feher, G. (2007) Protein-cofactor interactions in bacterial reaction centers from *Rhodobacter sphaeroides* R-26: II. Geometry of the hydrogen bonds to the primary quinone Q_A^- by H-1 and H-2 ENDOR spectroscopy. *Biophys. J. 92*, 671–682.
44. Ermler, U., Fritzsch, G., Buchanan, S. K., and Michel, H. (1994) Structure of the photosynthetic reaction-center from *Rhodobacter sphaeroides* at 2.65 angstrom resolution: Cofactors and protein-cofactor interactions. *Structure 2*, 925–936.
45. Xu, Q., and Gunner, M. R. (2002) Exploring the energy profile of the Q_A^- to Q_B electron transfer reaction in bacterial photosynthetic reaction centers: pH dependence of the conformational gating step. *Biochemistry 41*, 2694–2701.